Geomechanics and Engineering, *Vol. 40, No. 3 (2025) 193-204*
https://doi.org/10.12989/gae.2025.40.3.193

A machine learning approach for predicting the impact of normal fault ruptures on batter pile foundations

Mukhtiar Ali Soomro*, Zhu Ziqing, Sharafat Ali Darban and Zhen-Dong Cui

School of Mechanics and Civil Engineering, China University of Mining and Technology, Xuzhou, Jiangsu, 221116, P.R. China

(*Received September 29, 2024, Revised January 30, 2025, Accepted February 3, 2025*)

Abstract. Earthquake-induced fault ruptures present a considerable risk to structures, especially underground systems like pile foundations. Batter pile foundations, among the various foundation types, are commonly employed for their effectiveness in withstanding inclined forces. Therefore, it is crucial to comprehensively understand how batter pile groups respond to fault ruptures under diverse geotechnical conditions to enhance geoengineering practices. In this study, 3D numerical modeling was used to investigate the internal force and damage distribution mechanisms of different batter pile groups subjected to various normal fault ruptures. Additionally, five novel machine learning regression models (i.e. Light Gradient Boosting Machine (LightGBM), CatBoost, Extreme Gradient Boosting (XGBoost), ExtraTrees, and Random Forest (RF)) were developed to learn and predict the impact of four input parameters related to batter piles and normal fault ruptures. A database comprising 375 datasets was extracted from numerical modeling results to build the learning and testing framework. The comprehensive results indicate that LightGBM has the highest potential for estimating the internal force and concrete damage distribution along batter pile foundations due to normal faults. The coefficient of determination (R^2) exceeded 0.90 across all models, with reasonable values for mean square error (MSE), root mean square error (RMSE), and mean absolute error (MAE). This study provides an effective method for estimating the response of batter pile foundations to normal fault ruptures. The findings can assist engineers in designing batter pile foundations and evaluating the damage conditions of structures subjected to fault ruptures prior to detailed inspections.

Keywords: battered pile foundation; earthquake; fault rupture; machine learning

1. Introduction

Batter pile foundations are commonly utilized to counteract tilting and lateral movement in superstructures such as bridge piers and transmission towers. Despite their effectiveness in resisting horizontal forces and dynamic loads generated by earthquakes (Bharathi *et al.* 2019), post-seismic observations from several major earthquakes have revealed that pile foundations may be less effective than stiff mat foundations in safeguarding structures against significant fault ruptures occurring beneath them (Anastasopoulos *et al.* 2013, Huynh *et al.* 2021, Chou and lin, 2020). Additionally, many building codes and standards discourage the use of batter piles in seismic regions (Zheng *et al.* 2016) due to the large forces exerted on the pile cap, reduced bending capacity caused by axial forces, unfavorable cap rotations, and residual bending moments resulting from pre-earthquake soil settlement (Gerolymos *et al.* 2008).

Earthquake-induced fault ruptures often lead to significant ground displacements in multiple directions, posing severe risks to foundations. While extensive research has been conducted to understand the behavior of pile foundations under fault rupturing, the interaction between batter pile foundations and soil remains insufficiently explored. Centrifuge model studies and numerical simulations (Cai *et al*. 2016, Loli *et al*. 2011, Ahmed *et al*. 2009, Anastasopoulos *et al*. 2009) have been carried out to observe how fault ruptures interact with various types of pile foundations. Related studies on the interaction between soil movement and underground structures (Khanbabazadeh *et al*. 2023, Cui *et al*. 2023, Soomro *et al*. 2023, Jeon *et al*. 2023, Soomro *et al*. 2024) have also provided valuable insights. These studies indicate that tilting, deformation, and significant internal forces can severely compromise the bearing capacity of structures. However, the distinct impacts of normal and reverse fault ruptures on soil and pile foundations have not been extensively investigated.

In recent years, machine learning (ML) has emerged as a valuable tool in geotechnical engineering, offering innovative approaches for analyzing various geotechnical scenarios. For instance, XGBoost has been employed to model rock burst phenomena in deep tunnels, highlighting its potential for understanding and mitigating rock burst hazards (Mahmoodzadeh *et al*. 2022). In foundation design, ML has also been utilized to enhance understanding of shallow foundations and the response of pile groups to underground soil movement (Kim *et al*. 2024, Shubham *et al*. 2024). A wide range of ML models has been developed and extensively studied in recent years. Evaluations of different algorithms, including XGBoost, CatBoost, LightGBM, ExtraTrees, and Random Forest, have been conducted to assess their adaptability and predictive

*Corresponding author, Ph.D.
E-mail: eng.soomro@gmail.com

ISSN: 2005-307X (Print), 2092-6219 (Online)

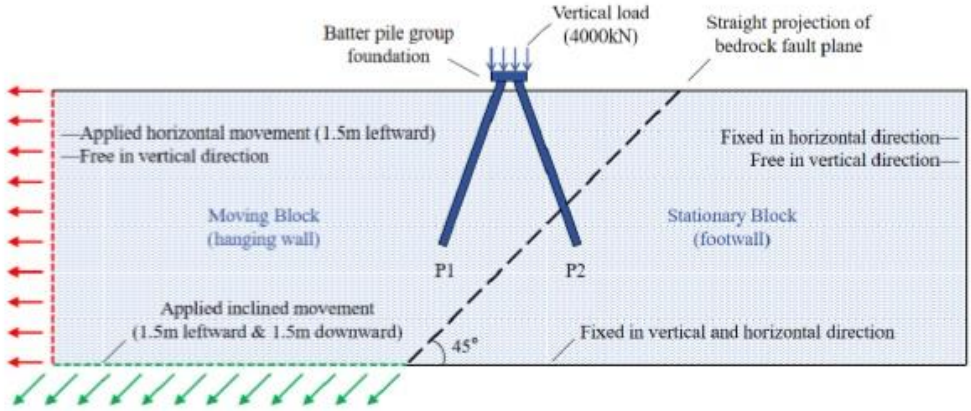

Fig. 1 Schematic representation of the generation of the normal fault rupture

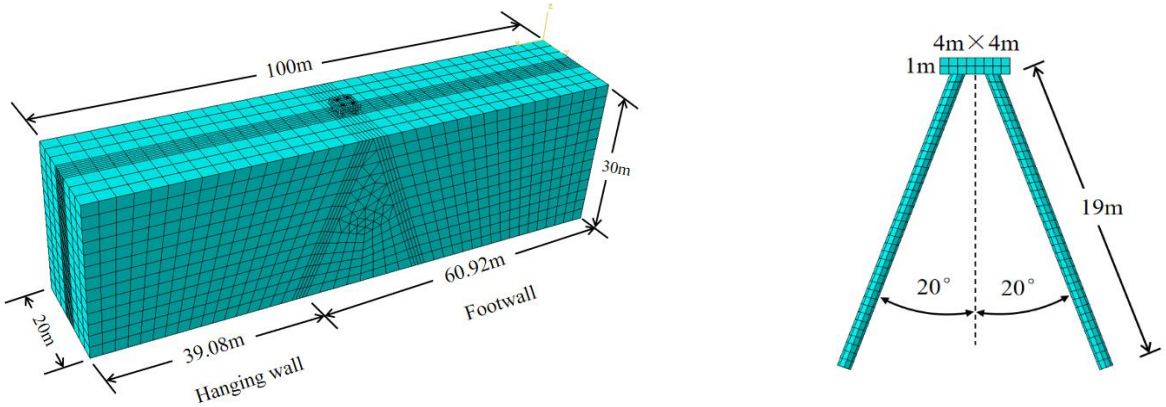

(a) (b)

Fig. 2 Finite element mesh of the numerical analysis: (a) overview (b) batter pile group foundation

accuracy (Shahani *et al*. 2022, Dashtgoli *et al*. 2024, Samadi *et al*. 2024). These models have demonstrated high effectiveness in generating accurate predictions and producing essential data for geoengineering applications, showcasing their potential for advancing research in the field. Among these algorithms, XGBoost has consistently delivered superior performance, making it a focus of this study alongside four other popular ML models.

Previous research has primarily examined the effects of fault ruptures on shallow or vertical pile foundations, leaving a gap in systematic studies on the behavior of batter pile groups subjected to vertical loads during the propagation of normal and reverse fault ruptures. This study aims to address this gap by investigating the deformation and failure mechanisms of batter pile groups under such conditions through 3D numerical modeling. Additionally, machine learning techniques are integrated into this research to identify key factors influencing the stability of batter pile groups, enabling geoengineers to design pile foundations with enhanced resistance to fault rupture hazards. The trained ML models further provide researchers with a novel approach to estimate the damage sustained by pile foundations due to fault ruptures.

Based on the prediction of the propagation of the faulting (Loukidis *et al.* 2009, Yao *et al.* 2020, Ebadi-Jamkhaneh *et al.* 2021), a batter pile foundation was placed near the developing path of the faulting plane as shown in the Fig. 2. The width and depth of soil mesh in analysis were taken as 20 m and 30 m. To simulate the soil movement induced by bedrock slip more realistically, the length of the soil along the faulting direction was taken as 100 m. The pile is discretized using 8-node linear brick

2. 3D finite element analysis

2.1 Description of geometry parameters and finite element mesh

The geometric parameters of the model are presented in the Fig. 1. The pile inclination angle was set to be 20° as which is now commonly used in constructions for having a higher working load capacity and stability (Al-Neami *et al.* 2016, Kim *et al.* 2021). In this study, the numerical model simulates a non-displacement pile, which closely resembles bored piles commonly used in practice. The installation

Table 1 Parameters of the hypoplastic model applied in the numerical simulations

	Parameters	Values	Units
1	ρ	1.6147×10^{3}	kg/m^3
2	k	8.64×10^{-5}	m/d
3	e	0.7	-
4	φ_c	22	degree
5	p_t	1	-
6	λ^*	0.095	-
7	κ^*	0.015	-
8	N	1.344	-
9	r_{lc}	0.5	-
10	$\dot{k}$	0	-
11	A	0	-
12	s_f	0	-
13	m_R	9	-
14	m_T	11	-
15	r_{uc}	0.00005	-
16	β_r	0.1	-
17	χ	1	-
18	K_w	0	-
19	p_{ref}	15	-

effects were not explicitly modeled; however, the initial stress state around the pile was carefully established to reflect realistic in situ conditions. Since bored piles are formed by excavation and subsequent concrete placement, they do not induce significant radial soil displacement during installation, making them appropriate for the numerical representation used in this study. This approach ensures that the initial stress distribution in the numerical model is consistent with the expected field conditions for non-displacement piles.

Based on the prediction of the propagation of the faulting (Loukidis *et al.* 2009, Yao *et al.* 2020, Ebadi-Jamkhaneh *et al.* 2021), a batter pile foundation was placed near the developing path of the faulting plane as shown in the Fig. 2. The width and depth of soil mesh in analysis were taken as 20 m and 30 m. To simulate the soil movement induced by bedrock slip more realistically, the length of the soil along the faulting direction was taken as 100 m. The pile is discretized using 8-node linear brick.

2.2 Constitutive model and model parameters used in numerical analyses

This research was conducted to simulated the interaction between batter pile group and clay induced by fault ruptures (normal and reverse) due to the movement of the underlying bedrock. The clay was applied in the model for the lower elastic modulus so that the foundation could endure severer soil movement before total structural failure than other stiffer soil like sand (Kumarn *et al.* 2015, Hazzar *et al.* 2023, Jiménez and Jenck 2022, Jaber *et al*. 2023). The

Table 2 Parameters of the CDP model applied in the numerical simulations

	Parameters	Values	Unit
1	ρ	2500	kg/m^3
2	E	31101	MPa
3	μ	0.2	-
4	α	38	degree
5	e	0.1	-
6	f_{b0}/f_{c0}	1.16	-
7	K	0.6666667	-
8	η	0.00001	-

numerical analyses presented herein were performed using the finite element software Abaqus, which is capable of applying hypoplastic model to simulate soil. One of the greatest advantages of hypoplastic model is the precision to simulate the small strain of clay, which is practical for this $\dot{\sigma} = f_s[L(\sigma, e)\colon \dot{\varepsilon} + f_d N(\sigma, e)\|\dot{\varepsilon}\|]$study (Masin *et al.* 2005, 2007). According to the formula summarized by Mašín (2005) the general form of the hypoplastic model is given as $L(\sigma, e)\colon \dot{\varepsilon}$Where $\dot{\sigma}$ denotes the stress ratio tensor; $\dot{\varepsilon}$ denotes the strain rate tensor; L and N are the fourth-order tensor function and the second-order tensor function representing the state of the soil body, respectively. is a linear term that indicates a linear increase in stress with respect to strain. The second part $(\sigma, e)\|\dot{\varepsilon}\|$ establishes a nonlinear relationship between the stress increment and the strain increment. The stiffness factor *fs*, which controls the effect of the mean effective stress, can be determined from isotropic compression, which reflects the influence of barotropy, and *fd*, which is a densification factor related to the pore ratio, which reflects the influence of pyknotropy. The corresponding values assigned to the input parameters of the constitutive model are shown in Table 1.

Behavior of reinforced concrete structures cannot be captured by elastic damage models or elastic-plastic constitutive laws only (Sümer *et al.* 2015). But applying a concrete damage plastic (CDP) model, which is the combination of the two models, can lead the researchers to observe the reinforced concrete structures thoroughly. In this research, concrete damage plastic model was applied to simulate the deformation and failure mechanism of the batter pile foundation. The parameters of the CDP model are shown in Table 2. Besides, the reinforcement bar group was also installed into the foundation to make the response of the foundation more reliable and practical.

In order to consider the interaction between soil and structures, specific properties related to tangential behaviour and normal behaviour are chosen for the contact between the battered piles and soil. The Coulomb Friction model is utilized to define frictional contact properties, enabling the simulation of tangential behaviour. On the other hand, the Hard Contact model is employed to replicate the nature of surface contact and simulate normal behaviour in Abaqus.

Table 3 An overview of the generated database

	Input				Output							
	D_p	S	θ_p	θ_f	M_1	M_2	L_{m1}	L_{m2}	d_{t1}	d_{t2}	d_{c1}	d_{c2}
Training set												
count	281	281	281	281	281	281	281	281	281	281	281	281
mean	0.799	0.885	19.96	66.28	0.532	0.573	0.198	0.46	0.89	0.675	0.146	0.092
std	0.163	0.419	7.183	13.983	0.257	0.354	0.177	0.133	0.136	0.314	0.144	0.15
min	0.6	0.3	10	45	0.151	0.059	0	0.132	0.03	0	0	0
25%	0.6	0.6	15	55	0.3	0.281	0.026	0.368	0.876	0.563	0.013	0
50%	0.8	0.9	20	65	0.501	0.5	0.211	0.447	0.948	0.811	0.104	0.014
75%	1.0	1.2	25	75	0.696	0.758	0.289	0.553	0.963	0.899	0.236	0.138
max	1.0	1.5	30	85	1.211	1.455	0.763	0.737	0.984	0.983	0.689	0.833
Testing set												
count	94	94	94	94	94	94	94	94	94	94	94	94
mean	0.804	0.945	20.11	61.17	0.549	0.608	0.198	0.468	0.894	0.632	0.156	0.101
std	0.165	0.438	6.723	13.923	0.275	0.389	0.19	0.121	0.121	0.349	0.152	0.171
min	0.6	0.3	10	45	0.155	0.075	0	0.158	0.345	0	0	0
25%	0.6	0.6	15	55	0.294	0.286	0.026	0.368	0.869	0.409	0.032	0
50%	0.8	0.9	20	65	0.501	0.486	0.211	0.447	0.948	0.797	0.106	0.015
75%	1.0	1.2	25	75	0.761	0.806	0.289	0.526	0.961	0.905	0.253	0.135
max	1.0	1.5	30	85	1.139	1.452	0.763	0.737	0.983	0.987	0.658	0.816

Note: D_p: pile diameter; S: fault slip distance; θ_p: pile inclination angle; θ_f: fault slip angle; M_1,M_2: maximum bending moment on P1,P2; L_{m1},L_{m2}: location of the maximum bending moment on P1,P2 (normalized pile length); d_{t1},d_{t2}: maximum tensile damage index on P1,P2; d_{c1},d_{c2}: maximum compression damage index on P1,P2

In this study, numerical modeling was employed to generate data required for assembling the database. As shown in Table 3, four parameters were identified as influential in the interaction between batter pile foundations and the surrounding soil: batter pile angle, fault propagation angle, pile diameter, and fault distance. These four parameters, considered as input variables, resulted in a total of 375 combinations (or samples). For each numerical simulation, the bending moment and concrete damage index distributions along the pile were extracted. These outputs are critical for evaluating the damage condition of batter pile structures. The data were then divided into two subsets: 75% of the samples were allocated to the training dataset, while the remaining 25% formed the testing dataset. This split was chosen to balance the risks of overfitting and underfitting. Stratified sampling was used to determine how the data were allocated between the training and testing datasets. This method ensures that the distribution of labels or categories remains consistent between the two subsets, allowing both the training and testing datasets to contain representative samples of each category. An overview of the generated database is provided in Table 3.

3. Interpretation of computed results

3.1 Induced soil movement and fault propagation

Fig. 3 depicts the displacement and shear strain distribution in the soil under normal and reverse faulting scenarios, respectively. Significant shear strain is observed in the bottom soil layer, corresponding to the initiation point of the fault plane. This strain results from the relative dislocation of the hanging wall and the footwall. The intensity of the shear strain diminishes as the fault plane extends upward. The dislocation of the hanging wall generates shear strain over a wide area surrounding the vertical projection of the bedrock fault plane and the batter pile foundation. This highlights the considerable impact of soil shear forces on the behavior of batter pile foundations. Differential settlement caused by faulting leads to uneven ground movement, tilting the pile cap and redistributing loads within the pile group. In normal faulting, settlement near the hanging wall increases axial forces on pile P2, resulting in greater penetration and pile deflection. Conversely, in reverse faulting, the uplift caused by the hanging wall creates oblique forces that shift additional loads to pile P1, causing significant bending and deflection along its length. The redistribution of loads in these scenarios alters the shaft resistance of individual piles. For example, normal faulting increases shaft friction near pile P2, whereas reverse faulting enhances load transfer to pile P1 due to oblique soil displacement. These changes in load transfer mechanisms, combined with localized shear strain around the pile toes and along the pile bodies, influence the overall structural stability and performance of the foundation system.

The shear strain patterns induced by normal and reverse faulting exhibit distinct differences. During normal faulting, the movement of the hanging wall tilts the pile cap, increasing the axial force on pile P2. Due to insufficient end-bearing capacity, pile P2 is driven deeper into the soil, generating significant shear strain around its toe. In contrast, during reverse faulting, shear strain concentrates around the toe of pile P1. As the pile cap tilts further, more load is transferred to pile P1. This, combined with the oblique and upward movement of

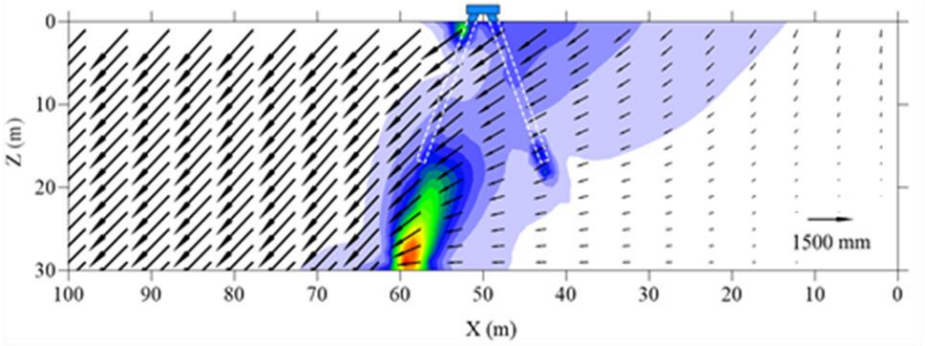

Fig. 3 Soil displacement vectors and shear strain contours due to normal faulting

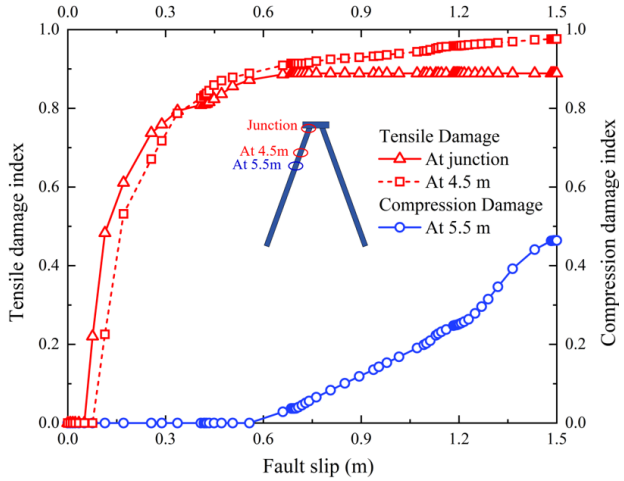

(a)

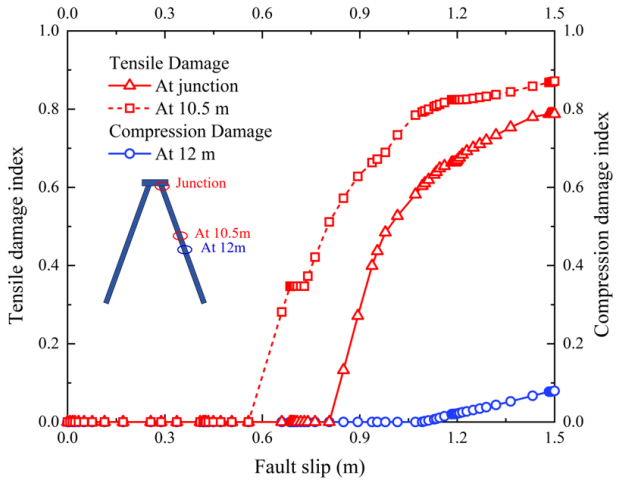

(b)

Fig. 4 Progressive damage factors during occurrence of normal fault rupture in piles (a) P1 and (b) P2

the surrounding soil, increases the axial force on pile P1. The insufficient end-bearing capacity ultimately leads to the failure of the soil structure around the toe of pile P1, propagating shear strain from the bottom soil layer to the toe of pile P1. Regarding soil displacement, it is noteworthy that the movement around pile P2 is nearly perpendicular to the pile body under both normal and reverse faulting conditions. In contrast, oblique soil displacement is observed along the body of pile P1. This oblique displacement increases the shaft resistance of pile P1, which subsequently affects its axial force.

3.2 Damage condition of the batter pile foundation

The damage conditions and deformation mechanisms of the batter pile foundation under normal faulting are illustrated in Figs. 4(a) and 4(b). Both piles P1 and P2 bent in the same

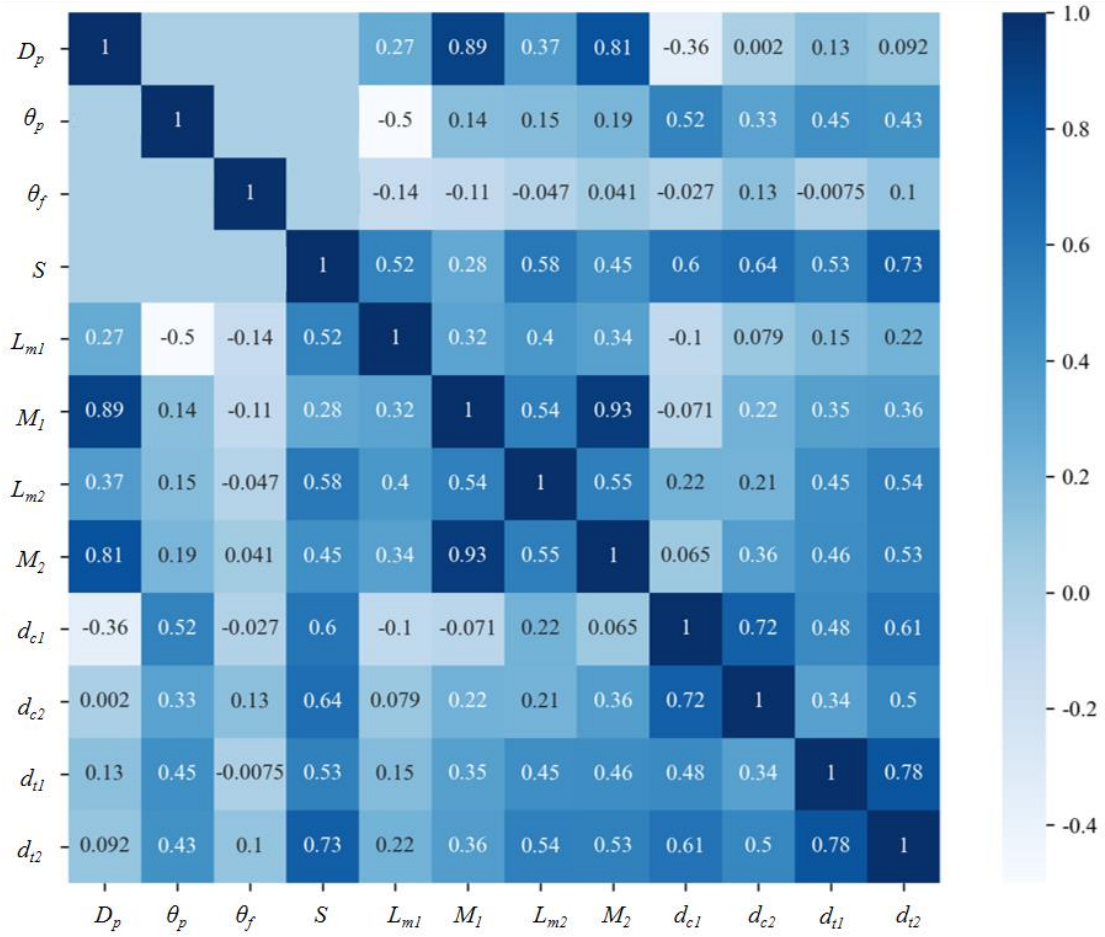

Fig. 5 Correlation heat map of all parameters in the database

direction during the fault rupture events, aligning with the tilting of the pile cap observed earlier. The batter pile foundations experienced significantly more tensile damage than compressive damage overall.

Severe damage was observed at the junctions between the piles and the pile cap, as anticipated based on prior studies. However, critical tensile damage was evident at these junctions, while no compressive damage was observed. For the pile shafts, tensile damage predominantly occurred along the right-side surfaces of both batter piles, whereas compressive damage was confined to small regions on the left-side surfaces during normal fault rupture. The tilting of the pile cap, influenced by fault-induced displacement and shear strain, caused uneven loading on the piles, increasing tensile forces on one side while inducing limited compression on the other., the tilting of the pile cap is a critical factor affecting the damage distribution. The differential displacement and shear strain contours in Fig. 3 demonstrate that soil movement amplifies tensile forces in specific regions of the piles. For instance, the oblique displacement of soil near pile P1 during normal faulting concentrates tensile forces on its right side, consistent with the observed damage. In contrast, the more uniform soil movement around pile P2 produces a distributed bending pattern, leading to tensile damage along its length but with minimal compressive damage. These findings reveal that the deformation and damage mechanisms of the batter pile foundation are strongly influenced by the interplay of fault-induced soil displacement, shear strain, and the tilting of the pile cap. The widespread tensile damage, particularly during normal faulting, underscores the vulnerability of the foundation to such seismic events, with the junctions and the right-side surfaces of the piles identified as critical regions.

4. Discussion on machine learning results

4.1 Damage condition of the batter pile foundation

To visualize the relationships between different parameters, the correlation heat map for the entire dataset is presented in Fig. 5. A correlation heat map is a visual representation of a correlation matrix, using colors and numerical values to depict the degree of correlation between variables. It is a two-dimensional data representation where the diagonal dark blue cells typically represent the correlation of a variable with itself, which is always 1. For two different variables, higher absolute values and deeper colors indicate stronger correlations. Positive values generally signify an increase in a relationship or quantity, while negative values indicate a decrease. As shown in the figure, the relationships among variables such as pile diameter (D_p), pile angle (θ_p), fault slip angle (θ_f), fault slip

Table 4 The statistical parameters computed to evaluate the efficiency of the ML models

	M_1	M_2	L_{m1}	L_{m2}	d_{t1}	d_{t2}	d_{c1}	d_{c2}
LGBM								
R^2	0.9910	0.9883	0.8340	0.7751	0.9361	0.9747	0.9139	0.9257
MSE	0.0013	0.0008	0.0059	0.0032	0.0009	0.0030	0.0019	0.0021
RMSE	0.0369	0.0297	0.0772	0.0572	0.0305	0.0554	0.0445	0.0465
MAE	0.0300	0.0218	0.0539	0.0402	0.0205	0.0315	0.0296	0.0262
CatBoost								
R^2	0.9948	0.9897	0.6728	0.8038	0.8648	0.9555	0.9307	0.9070
MSE	0.0007	0.0007	0.0117	0.0028	0.0019	0.0054	0.0015	0.0027
RMSE	0.0278	0.0278	0.1084	0.0534	0.0444	0.0735	0.0399	0.0521
MAE	0.0200	0.0200	0.0741	0.0354	0.0239	0.0426	0.0242	0.0521
XGBoost								
R^2	0.9894	0.9762	0.7306	0.8004	0.8283	0.9453	0.9083	0.8386
MSE	0.0016	0.0017	0.0096	0.0029	0.0025	0.0066	0.0021	0.0047
RMSE	0.0400	0.0423	0.0984	0.0539	0.0501	0.0816	0.0459	0.0686
MAE	0.0313	0.0314	0.0682	0.0395	0.0325	0.0484	0.0286	0.0435
ExtraTrees								
R^2	0.9903	0.9774	0.6736	0.7684	0.8598	0.9427	0.9312	0.9006
MSE	0.0014	0.0016	0.0117	0.0033	0.0020	0.0069	0.0015	0.0029
RMSE	0.0383	0.0412	0.1083	0.0580	0.0452	0.0835	0.0398	0.0538
MAE	0.0284	0.0291	0.0728	0.0580	0.0323	0.0404	0.0247	0.0270
RandomForest								
R^2	0.8930	0.9791	0.6414	0.7995	0.8698	0.9386	0.9199	0.8713
MSE	0.0162	0.0015	0.0128	0.0029	0.0019	0.0074	0.0018	0.0037
RMSE	0.1272	0.0396	0.1135	0.0540	0.0436	0.0864	0.0429	0.0612
MAE	0.1107	0.0301	0.0791	0.0380	0.0233	0.0543	0.0276	0.0269

distance (S), the location of maximum bending moments in piles P1 and P2 (L_{m1} and L_{m2}), maximum bending moments (M_1 and M_2), and the compression and tensile damage indices of key points on the piles (d_{c1}, d_{c2}, d_{t1}, and d_{t2}) are demonstrated.

The pile diameter (D_p) shows a strong positive correlation with the maximum bending moments (M_1 and M_2) in both piles (0.89 and 0.81, respectively). Specifically, larger pile diameters lead to higher bending moments in the piles. However, there is little correlation between pile diameter and the damage condition of the pile body, suggesting that increasing pile diameter may not be an effective strategy for mitigating fault rupture hazards. Similarly, the pile angle (θ_p) exhibits a strong positive correlation with the damage indices of the pile body, indicating that high oblique pile angles are not advisable in earthquake-prone regions. As expected, the fault slip distance (S) shows positive correlations with both the bending moments and the damage levels along the piles. This implies that longer fault slips tend to cause greater damage to batter pile foundations. However, the influence of the fault slip angle (θ_f) on pile response is less significant compared to other factors. This contrasts with the stronger impact observed for the pile angle (θ_p).

To thoroughly evaluate the predictive performance of the five machine learning models, key regression model parameters are summarized in Table 4. Overall, the predictions for the maximum bending moments (M_1 and M_2) performed best. Due to the application of the concrete damage plasticity (CDP) model to the batter piles, the tensile and compression damage patterns in the pile body proved more challenging to predict. Nonetheless, these predictions achieved coefficients of determination (R^2) exceeding 0.9. However, the location of the maximum bending moment showed some variability due to stress redistribution caused by concrete damage, resulting in an R^2 of around 0.8. Additionally, the evaluation metrics, including mean squared error (MSE), root mean squared error (RMSE), and mean absolute error (MAE), were all significantly lower than the variance of their predicted variables, demonstrating satisfactory prediction performance.

Fig. 6 provides a representation of the prediction performance of the machine learning (ML) methods, selected based on the coefficient of determination (R^2). These plots clearly illustrate that the distribution of the predicted results closely aligns with the computed results. The x-coordinates of the blue scatter points represent the computed values from Abaqus, while the y-coordinates represent the prediction values from the ML models. The closer the scatter points are to the green regression line (slope = 1), the better the prediction performance of the ML model.

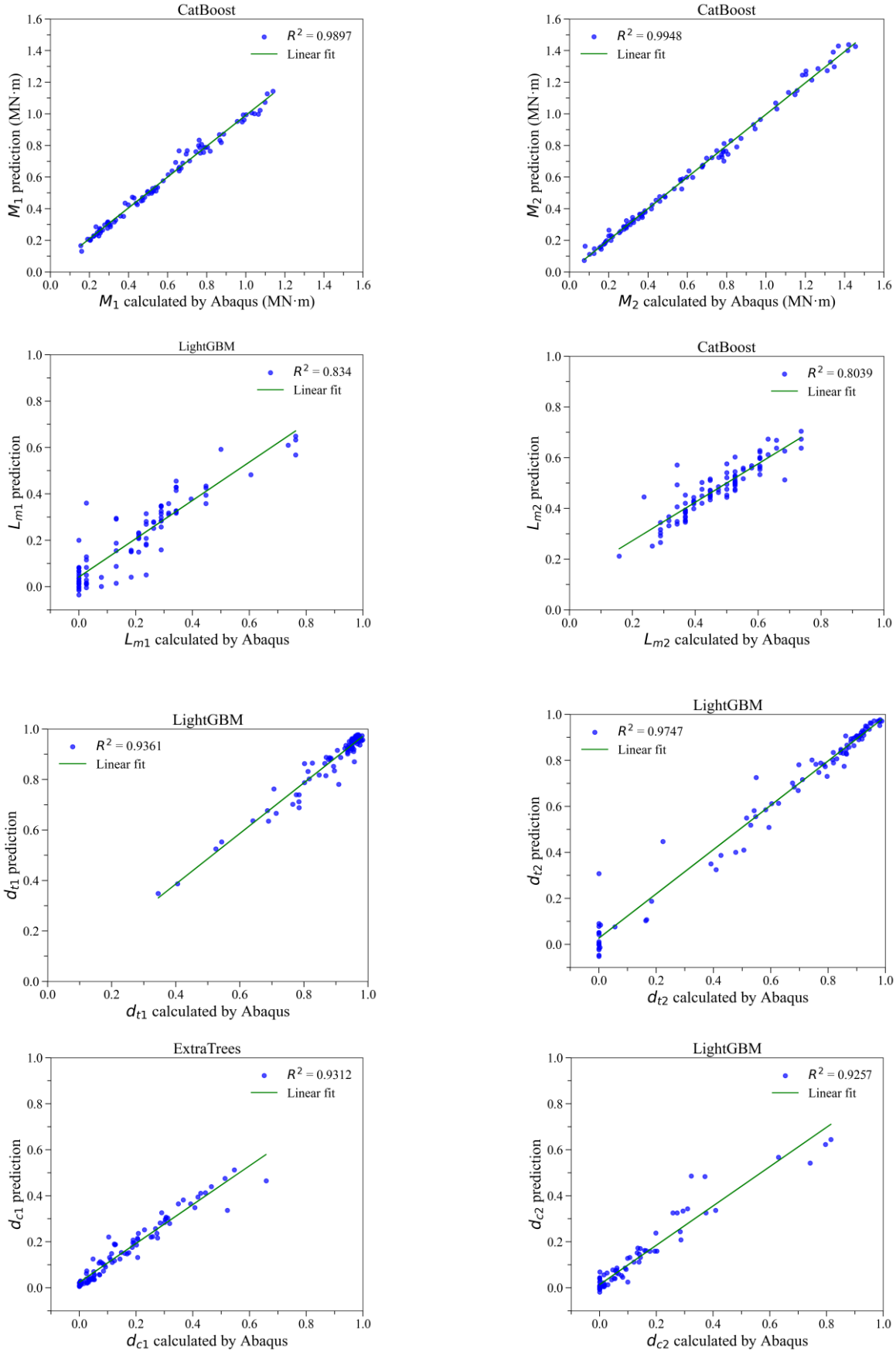

Fig. 6. Predictions of the selected ML models are compared with the calculations of computed results using the scatter plots

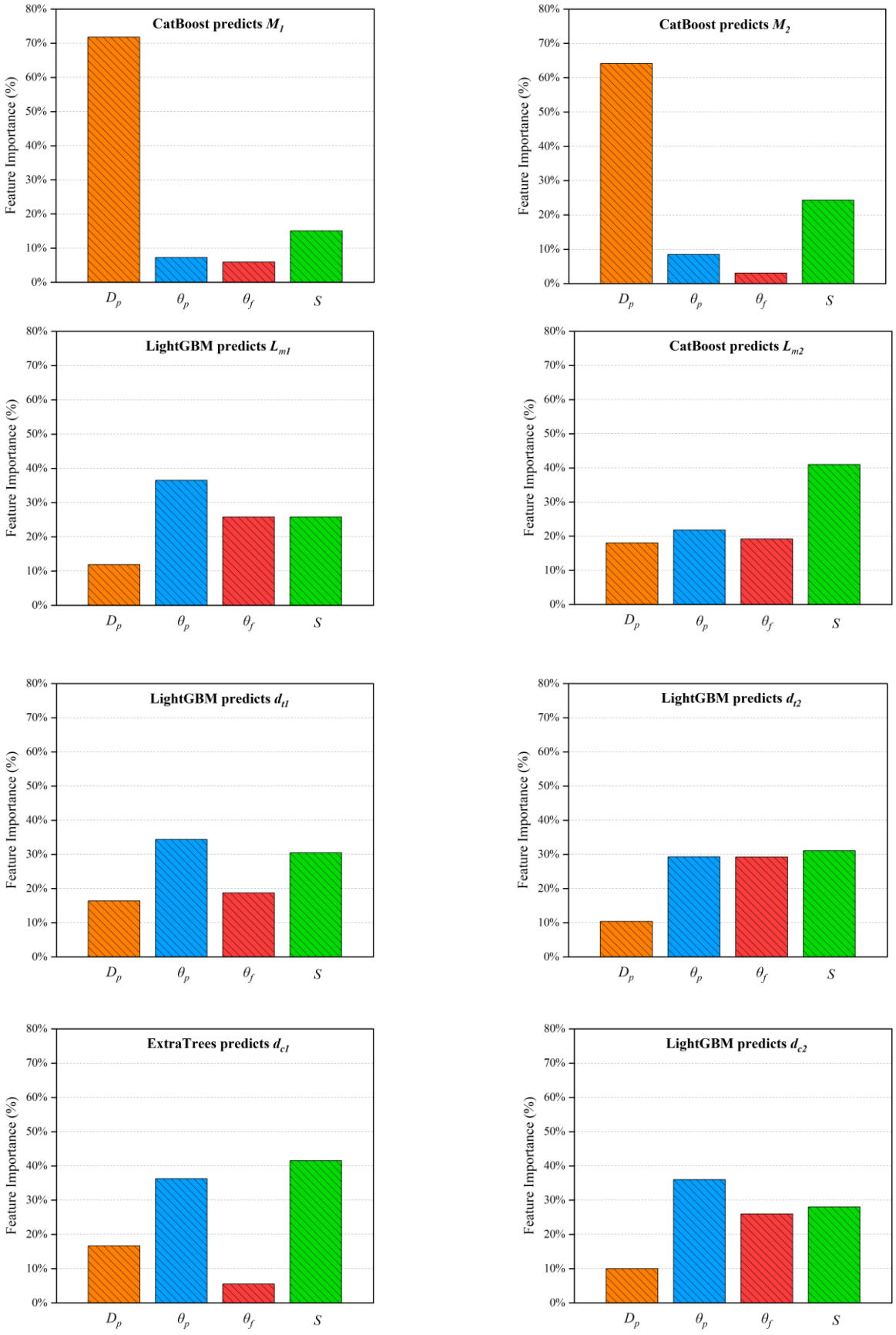

Fig. 7 Predictions of the selected ML models are compared with the calculations of computed results using the scatter plots

The prediction results for the maximum bending moments of both piles (M_1 and M_2) demonstrate an excellent R^2 value of 0.99, indicating strong agreement between the computed results and the predictions made by the CatBoost model. Overall, considering the ML evaluation parameters presented in Table 4, the maximum bending moment along the piles is most accurately estimated by the CatBoost model. Meanwhile, the locations of maximum bending moments (Lm1 and Lm2) and the concrete tensile and compression damage indices (d_{c1}, d_{c2}, d_{t1}, and d_{t2}) are better predicted with higher precision by the LightGBM model. The scatter plots in the figure reveal more than just ML performance; they also highlight the distribution patterns of the variables.

For instance, the maximum bending moment on P2 is often higher than that on P1, and their respective locations are not identical. Most of the maximum bending moments occur near the shallower regions of the piles, closer to the pile cap. However, for P2, these moments are more concentrated in the middle region (the values of L_{m1} and L_{m2} represent normalized pile lengths, where 0 corresponds to the pile cap and 1.0 to the pile toe). Furthermore, tensile damage on P1 is significantly more severe than on P2, while compression damage on both piles is generally milder compared to tensile damage.

To clarify the impact of each feature on the model predictions and understand the basis for the model's decisions, feature importance diagrams are presented in Fig. 7. These diagrams indicate that pile diameter (D_p) is the most influential input variable for predicting the maximum bending moment along the pile body, accounting for approximately 70% of the feature importance. Other variables have considerably less impact in comparison. However, the influence of D_p diminishes (below 20%) when predicting the location of the maximum bending moments (L_m) and the concrete damage indices. In these cases, the pile inclination angle (θ_p) and fault slip distance (S) become the key features, with the highest feature importance values reaching around 30%.

Additionally, the feature importance of θ_p is consistently higher than that of θ_f. This observation aligns with the heat map in Fig. 5, where the correlation matrix values for θ_p are consistently higher in absolute terms than those for θ_f. The fault slip angle (θ_f) describes the angle of the straight projection line of the underlying bedrock fault plane, which controls soil movement around the pile foundation. However, given the maximum fault slip distance of 1.5 m in a 30 m deep soil layer, the impact of the fault slip angle is relatively minor. Nonetheless, the feature importance of S remains significant, leading to the conclusion that when a fault rupture occurs in deep soil with a relatively short fault slip distance, the fault slip distance has a greater influence on the response of foundation structures than the fault slip angle.

5. Practical implications and design recommendations for seismic regions

The findings of this study offer critical insights into the design and performance optimization of batter pile foundations under fault rupture scenarios. Specific engineering implications and actionable design recommendations are summarized as follows.

5.1 Mitigation of tensile damage in batter piles

This study highlights that batter piles are particularly susceptible to tensile damage caused by differential loading and displacement during normal and reverse faulting. To mitigate these vulnerabilities, several strategies are recommended. Firstly, high-tensile-strength materials should be utilized in the upper sections of the pile shafts and at their junctions with the pile cap. These regions experience the highest tensile stresses during seismic events, and reinforcing them can significantly enhance the piles' ability to withstand tensile forces, thereby improving overall structural integrity. Secondly, the design of pile-to-cap connections should be strengthened with ductile materials and energy-dissipating mechanisms. These improvements will enable the connections to better accommodate the significant bending moments and shear forces observed during fault ruptures. As a result, the likelihood of damage will be reduced, and the resilience of the foundation system will be improved.

5.2 Enhancing load distribution and reducing tilting

Fault-induced soil movements result in uneven load distribution among the piles, leading to cap tilting and structural instability. To mitigate these issues, engineers can adopt targeted design strategies to enhance foundation performance. One effective approach is to adjust the spatial arrangement of batter piles to optimize load sharing and reduce differential settlement, thereby improving the overall stability of the pile group. Furthermore, increasing the rigidity of the pile cap can significantly reduce tilting by ensuring more even load redistribution across the pile group. These combined measures effectively mitigate the adverse effects of fault-induced movements, promoting a more stable and resilient foundation system.

5.3 Design adaptations for specific faulting scenarios

Normal faulting often causes deeper penetration and localized damage in specific piles, posing significant stability challenges. To address this, employing larger end-bearing pile tips can enhance load distribution and reduce the risk of failure. Additionally, soil improvement techniques near critical pile toes can strengthen the surrounding soil, thereby mitigating excessive deformation and enhancing overall stability. In contrast, reverse faulting generates uplift forces and oblique movements that compromise the structural integrity of pile foundations. To counteract these effects, pile shafts can be pre-tensioned or equipped with anchor systems specifically designed to resist upward displacements. These measures ensure greater resilience against the unique challenges posed by reverse faulting scenarios.

5.4 Recommendations for monitoring and maintenance

Regular inspection and monitoring of pile foundations in seismic regions are crucial for ensuring structural safety. Integrating embedded sensors to monitor stress distribution and displacement provides real-time data, enabling the early detection of potential vulnerabilities. This proactive approach facilitates timely interventions to mitigate risks and maintain foundation stability.

6. Conclusions

This study presents findings from numerical modeling tests that explore the interaction between batter piles and surrounding soil under the influence of normal faulting. Furthermore, five innovative machine learning regression models—Light Gradient Boosting Machine (LightGBM), CatBoost, Extreme Gradient Boosting (XGBoost), ExtraTrees, and Random Forest (RF)—were developed to analyze and predict the effects of four key parameters related to batter piles and normal fault ruptures. The outcomes of the numerical modeling and machine learning analyses lead to the following conclusions:

(1) Normal faulting caused more significant displacement and tilting of the pile cap than reverse faulting. For the same fault slip distance, normal faulting resulted in a 10.7% tilt and 0.94 meters of settlement. To address these effects, pile cap designs should include features that can resist increased tilting forces, such as reinforced connections or distributed support systems.

(2) Tensile damage occurred earlier and was more pronounced than compressive damage under both normal and reverse fault ruptures. To enhance the structural integrity of batter pile foundations, reinforcing pile shafts and junctions with stronger steel bars or advanced composite materials would be effective, particularly against tensile stresses.

(3) CatBoost provided the best prediction for maximum bending moments (M_1 and M_2), achieving a determination coefficient (R^2) of over 0.9. LightGBM, on the other hand, offered more accurate predictions for the location of maximum bending moments (Lm1 and Lm2) and concrete tensile and compressive damage indexes (d_{c1}, d_{c2}, d_{t1}, and d_{t2}).

(4) The maximum bending moment typically occurs in the shallower regions of pile P1, closer to the pile cap, while in pile P2, the maximum bending moment is more concentrated toward the middle section.

(5) Pile diameter (D_p) is the most significant factor influencing the maximum bending moment in the pile body, showing a strong positive correlation with M_1 and M_2 for both piles. This indicates that larger pile diameters may lead to higher bending moments during fault rupture development.

(6) Pile angle (θ_p) shows a strong positive correlation with pile body damage indexes, suggesting that steep pile angles should be avoided in earthquake-prone areas.

(7) Fault slip distance (S) exhibited positive correlations with both bending moment and damage degree along the piles, as expected. Fault ruptures with longer slip distances are likely to cause more severe structural damage.

Acknowledgements

The authors express their gratitude for the financial assistance provided by China University of Mining and Technology, Xuzhou, China PR.

References

Ahmed, W. and Bransby, M.F. (2009), "Interaction of shallow foundations with reverse faults", *J. Geotech. Geoenviron. Eng.*, **135**(7), 914-924. **135**(7), https://doi.org/10.1061/(ASCE)GT.1943-5606.000007.

Al-Neami, M.A., Rahil, F.H. and Al-Bayati, K.S. (2016), "Bearing capacity of batter piles embedded in sandy soil", *Int. J. Geotech. Eng.*, **10**(5), 529-532. https://doi.org/10.1080/19386362.2016.1203094.

Anastasopoulos, G., Gazetas, G. and Bransby, M.F. (2009), "Normal fault rupture interaction with strip foundations", *J. Geotech. Geoenviron. Eng.*, **135**(3), 359-370. https://doi.org/10.1061/(ASCE)1090-0241(2009)135:3(359).

Anastasopoulos, I., Kourkoulis, R., Gazetas, G. and Tsatsis, A. (2013), "Interaction of piled foundation with a rupturing normal fault", *Geotechnique*, **63**(12), 1042-1059. https://doi.org/10.1680/geot.12.P.114.

Bharathi, B., Dubey, R.N. and Shukla, S.K. (2019), "Experimental investigation of vertical and batter pile groups subjected to dynamic loads", *Soil Dyn. Earthq. Eng.*, **116**, 107-119. https://doi.org/10.1016/j.soildyn.2018.10.012.

Cai, Q.P. and Ng, C.W.W. (2016), "Centrifuge modeling of pile-sand interaction induced by normal faulting", *J. Geotech. and Geoenviron. Eng.*, **142**(10), 04016046. https://doi.org/10.1061/(ASCE)GT.1943-5606.0001500.

Chou, J.C. and Lin, E.G.E. (2020), "Incorporating ground motion effects into Sasaki and Tamura prediction equations of liquefaction-induced uplift of underground structures", *Geomech. Eng.*, **22**(1), 25-33. https://doi.org/10.12989/gae.2020.22.1.025.

Cui, Z., Wang, T., Sheng, Q. and Zhou, G. (2023). "Investigation of the behavior of a tunnel subjected to strike-slip fault rupture with experimental approach", *Geomech. Eng.*, **33**(5), 477-486. https://doi.org/10.12989/gae.2023.33.5.477.

Dashtgoli, D.S., Dehnad, M.H., Mobinipour, S.A. and Giustiniani, M. (2024), "Performance comparison of machine learning algorithms for maximum displacement prediction in soldier pile wall excavation", *Undergr. Sp.*, **16**, 301-313. https://doi.org/10.1016/j.undsp.2023.09.013.

Ebadi-Jamkhaneh, M., Homaioon-Ebrahimi, A., Kontoni, D.P.N. and Shokri-Amiri, M. (2021), "Numerical FEM assessment of soil-pile system in liquefiable soil under earthquake loading including soil-pile interaction", *Geomech. Eng.*, **27**(5), 465-479. https://doi.org/10.12989/gae.2021.27.5.465.

Gerolymos, N., Giannakou, A. and Anastasopoulos, I. (2008), "Evidence of beneficial role of inclined piles: observations and summary of numerical analyses", *Bull. Earthq. Eng.*, 705-722. https://doi.org/10.1007/s10518-008-9085-2.

Hazzar, L., Hussien, M.N. and Karray, M. (2023), "Numerical investigation of the lateral response of battered pile foundations", *Int. J. Geotech. Eng.*, **11**(4) , 376-392. https://doi.org/10.1080/19386362.2016.1224030.

Huynh, V.Q., Nguyen, T.K. and Nguyen, X.H. (2021), "Seismic analysis of soil-structure interaction: Experimentation and modeling", *Geomech. Eng.*, **27**(2), 115-121. https://doi.org/10.12989/gae.2021.27.2.115.

Jaber, L., Mezeh, R., Zein, Z., Azab, M. and Sadek, M. (2023), "Nonlinear numerical analysis of influence of pile inclination on

the seismic response of soil-pile-structure system", *Geomech. Eng.*, **34**(4), 437-447. https://doi.org/10.12989/gae.2023.34.4.437.

Jiménez, G.A.L., Dias, D. and Jenck, O. (2022), "Seismic loading response of piled systems on soft soils - Influence of the Rayleigh damping", *Geomech. Eng*., **29**(2), 155-170. https://doi.org/10.12989/gae.2022.29.2.155.

Jeon, Y. and Lee, C.J. (2023). "Analysis of pile group behaviour to adjacent tunnelling considering ground reinforcement conditions with assessment of stability of superstructures", *Geomech. Eng.*, **33**(5), 463-475. https://doi.org/10.12989/gae.2023.33.5.463.

Khanbabazadeh, H. and Mert, A.C. (2023), "Response of steel pipeline crossing strike-slip fault in clayey soils by nonlinear analysis method", *Geomech. Eng.*, **34**(4), 409-424. https://doi.org/10.12989/gae.2023.34.4.409.

Kim, J., Yun, S.K., Kang, M. and Kang, G. (2021), "Behavior characteristics of single batter pile under vertical load", *Appl. Sci.*, **11**(10), 4432. https://doi.org/10.3390/app11104432.

Kim, S.B., Oh, D.W., Cho, H.J. and Lee, Y.J. (2024), "Investigation of pile group response to adjacent twin tunnel excavation utilizing machine learning", *Geomech. Eng*., **38**(5), 517-528. https://doi.org/10.12989/gae.2024.38.5.517.

Kumarn, J. and Chakraborty, M. (2015), "Bearing capacity of a circular foundation on layered sand-clay media", *Soils Found.*, **55**(5), 1058-1068. https://doi.org/10.1016/j.sandf.2015.09.008.

Loli, M., Anastasopoulos, I. and Bransby, M.F. (2011), "Caisson foundations subjected to reverse fault rupture: Centrifuge testing and numerical analysis", *J. Geotech. Geoenviron. Eng.*, **137**(10), 914-925. https://doi.org/10.1061/(ASCE)GT.1943-5606.00005.

Loukidis, D., Bouckovalas, G.D. and Papadimitriou, A.G. (2009), "Analysis of fault rupture propagation through uniform soil cover", *Soil Dyn. Earthq. Eng*., **29**(11-12), 1389-1404. https://doi.org/10.1016/j.soildyn.2009.04.003.

Mahmoodzadeh, A., Nejati, H.R., Mohammadi, M., Mohammed, A.S., Ibrahim, H.H. and Rashidi, S. (2022), "Numerical and machine learning modeling of hard rock failure induced by structural planes around deep tunnels", *Eng. Fract. Mech*., **271**, 108648. https://doi.org/10.1016/j.engfracmech.2022.108648.

Mašín, D. (2005), "A hypoplastic constitutive model for clays", *Int. J. Numer. Anal. Method. Geomech*., **29**(4), 311-336. https://doi.org/10.1002/nag.416.

Samadi, H., Alanazi, A., Muhodir, S.H., Alsubai, S., Alqahtani, A., and Marzougui, M. (2024), "In-depth exploration of machine learning algorithms for predicting sidewall displacement in underground caverns", *Geomech. Eng*., **37**(4), 307-321. https://doi.org/10.12989/gae.2024.37.4.307.

Shahani, N.M., Zheng, X., Guo, X. and Wei, X. (2022), "Machine learning-based intelligent prediction of elastic modulus of rocks at thar coalfield", *Sustainability*, **14**(6), 3689. https://doi.org/10.3390/su14063689.

Shubham, K., Metya, S. and Sinha, A.K. (2024), "Optimizing shallow foundation design: A machine learning approach for bearing capacity estimation over cavities", *Geomech. Eng*., **37**(6), 629-641. https://doi.org/10.12989/gae.2024.37.6.629.

Soomro, M.A., Mangi, N., Mangnejo, D.A. and Zhang, Z. (2023), "The responses of battered pile to tunnelling at different depths relative to the pile length", *Geomech. Eng.*, **35**(6), 603-615. https://doi.org/10.12989/gae.2023.35.6.603.

Soomro, M.A., Zhu, Z., Aslam, M.S., Bilal, H., Yahya, A. and Badruddin, I.A. (2025), "3D numerical modeling of the deformation and failure mechanisms of batter pile groups subjected to fault ruptures", *Scientific Reports*, **15**(1), 2988. https://doi.org/10.1038/s41598-024-83044-9.

Sümer, Y. and Aktaş, M. (2015), "Defining parameters for concrete damage plasticity model", *Challenge J. Struct. Mech.*, **3**, 149-155. https://doi.org/10.20528/cjsmec.2015.07.023.

Yao, C. and Takemura, J. (2020), "Centrifuge modeling of single piles in sand subjected to dip-slip faulting", *J. Geotech Geoenviron. Eng.*, **146**(3), 04020001. https://doi.org/10.1061/(ASCE)GT.1943-5606.000220.

Zheng, L., Escoffier, S. and Kotronis, P. (2016), "Centrifuge modeling of batter pile foundations under earthquake excitation", *Soil Dyn. Earthq. Eng.*, **88**, 176-190. https://doi.org/10.1016/j.soildyn.2016.05.013.

GC